Journal Pre-proof

Evaluating mechanical and surface properties of zirconia-containing composites: 3D printing, subtractive, and layering techniques

Luiza Freitas Brum Souza, Kétlin Fagundes Teixeira, Ana Carolina Cadore-Rodrigues, Telma de Souza Pires, Luiz Felipe Valandro, Rafael R. Moraes, Mutlu Özcan, Gabriel Kalil Rocha Pereira

PII: S1751-6161(24)00240-6

DOI: https://doi.org/10.1016/j.jmbbm.2024.106608

Reference: JMBBM 106608

To appear in: *Journal of the Mechanical Behavior of Biomedical Materials*

Received Date: 5 March 2024

Revised Date: 1 May 2024

Accepted Date: 29 May 2024

Please cite this article as: Souza, L.F.B., Teixeira, K.F., Cadore-Rodrigues, A.C., Pires, T.d.S., Valandro, L.F., Moraes, R.R., Özcan, M., Pereira, G.K.R., Evaluating mechanical and surface properties of zirconia-containing composites: 3D printing, subtractive, and layering techniques , *Journal of the Mechanical Behavior of Biomedical Materials*, https://doi.org/10.1016/j.jmbbm.2024.106608.

Original research article – JMBBM

Evaluating mechanical and surface properties of zirconia-containing composites: 3D printing, subtractive, and layering techniques

Luiza Freitas Brum Souza[a], Kétlin Fagundes Teixeira[a], Ana Carolina Cadore-Rodrigues[a], Telma de Souza Pires[b], Luiz Felipe Valandro[ab], Rafael R. Moraes[c], Mutlu Özcan[d], Gabriel Kalil Rocha Pereira[ab]

[a] MSciD and PhD Post-Graduate Program in Oral Science, Faculty of Dentistry, Federal University of Santa Maria (UFSM), Santa Maria, Rio Grande do Sul State, Brazil.

[b] Faculty of Dentistry, Federal University of Santa Maria (UFSM), Santa Maria, Rio Grande do Sul State, Brazil.

[c] School of Dentistry, Universidade Federal de Pelotas, Pelotas, RS, Brazil

[d] Clinic for Masticatory Disorders and Dental Biomaterials, Center for Dental Medicine, University of Zurich, 8032, Zurich, Switzerland.

***Corresponding author:** *D.D.S, M.S.D., Ph.D., Adjunct Professor Gabriel Kalil Rocha Pereira, Prosthodontics Unit, Faculty of Odontology and Head of MsciD-PhD Graduate Program in Oral Science, Federal University of Santa Maria. Roraima Avenue #1000, T Street, Building 26F, Room 2383. Santa Maria, Rio Grande do Sul, Brazil. Zip-Code: 97.105-900. E-mail: gabriel.pereira@ufsm.com.*

Authors' e-mail addresses and contributions:

Luiza Freitas Brum Souza (luizafbrum@hotmail.com): Conceptualization; Data curation; Formal analysis; Investigation; Validation; Visualization; Writing – original draft; Writing – review & editing;

Kétlin Fagundes Teixeira (ketlinfteixeira@gmail.com): Data curation; Formal analysis; Investigation; Writing – review & editing;

Ana Carolina Cadore Rodrigues (anacadorerodrigues@gmail.com): Conceptualization; Data curation; Formal analysis; Investigation; Writing – review & editing;

Telma de Souza Pires (telma.pires@acad.ufsm.br): Data curation; Formal analysis; Investigation; Writing – review & editing;

Luiz Felipe Valandro (valandrolf@gmail.com): Formal analysis; Investigation; Methodology; Visualization; Writing - review & editing;

Rafael R. Moraes (moraesrr@gmail.com): Formal analysis; Investigation; Methodology; Visualization; Writing - review & editing;

Mutlu Özcan (mutluozcan@hotmail.com): Formal analysis; Investigation; Methodology; Visualization; Writing - review & editing;

Gabriel Kalil Rocha Pereira (gabriel.pereira@ufsm.com): Conceptualization; Data curation; Formal analysis; Funding acquisition; Investigation; Methodology; Project administration; Resources; Software; Supervision; Validation; Visualization; Writing - original draft; Writing - review & editing.

Running title: Mechanical behavior of 3D printed zirconia-containing resin composite

Abstract

This study assessed the monotonic and fatigue flexural strength (*FS*), elastic modulus (*E*), and surface characteristics of a 3D printed zirconia-containing resin composite compared to subtractive and conventional layering methods. Specimens, including discs (n= 15; Ø= 15 mm × 1.2 mm) and bars (n= 15; 14 × 4 × 1.2 mm), were prepared and categorized into three groups: 3D printing (3D printing – PriZma 3D Bio Crown, Makertech), Subtractive (Lava Ultimate blocks, 3M), and Layering (Filtek Z350 XT, 3M). Monotonic tests were performed on the discs using a piston-on-three-balls setup, while fatigue tests employed similar parameters with a frequency of 10 Hz, initial stress at 20 MPa, and stress increments every 5,000 cycles. The *E* was determined through three-point-bending test using bars. Surface roughness, fractographic, and topographic analyses were conducted. Statistical analyses included One-way ANOVA for monotonic *FS* and roughness, Kruskal-Wallis for *E*, and Kaplan-Meier with post-hoc Mantel-Cox and Weibull analysis for fatigue strength. Results revealed higher monotonic strength in the Subtractive group compared to 3D printing (p= 0.02) and Layering (p= 0.04), while 3D Printing and Layering exhibited similarities (p= 0.88). Fatigue data indicated significant differences across all groups (3D Printing < Layering < Subtractive; p= 0.00 and p= 0.04, respectively). Mechanical reliability was comparable across groups. 3D printing and Subtractive demonstrated similar *E*, both surpassing Layering. Moreover, 3D printing exhibited higher surface roughness than Subtractive and Layering (p< 0.05). Fractographic analysis indicated that fractures initiated at surface defects located in the area subjected to tensile stress concentration. A porous surface was observed in the 3D Printing group and a more compact surface in Subtractive and Layering methods. This study distinguishes the unique properties of 3D printed resin when compared to conventional layering and subtractive methods for resin-based materials. 3D printed shows comparable monotonic strength to layering but lags behind in fatigue strength, with subtractive resin demonstrating superior performance. Both 3D printed and subtractive exhibit similar elastic moduli, surpassing layering. However, 3D printed resin displays higher surface roughness compared to subtractive and layering methods. The study suggests a need for improvement in the mechanical performance of 3D printed material.

Keywords: 3D-printed dental resin. Resin composite. Dental Materials. Elastic modulus. Fatigue performance. Flexural strength. Prosthodontics.

Highlights

- 3D printed resin composite showed similar monotonic strength to the layering technique.
- 3D printed composite had lower monotonic strength compared to the subtractive technique.
- 3D printed composite exhibited lower fatigue strength than both subtractive and layering techniques.
- 3D printed composite had a rougher surface than those produced by subtractive and layering techniques.
- Mechanical performance of 3D printed materials requires improvement.

1 Introduction

Dental resin composites have become widely adopted as preferred restorative material in contemporary modern minimally invasive prosthodontics (Schlichting et al., 2022; Edelhoff et al., 2023). Their advantages over traditional glass-ceramics include lower abrasiveness toward opposing teeth (Kunzelmann et al., 2001), better absorption of functional stresses (Magne et al., 2002), and superior handling characteristics, such as the ability of intra-oral repairs (Schlichting et al., 2022). Research has shown that ultra-thin bonded resin composite restorations possess satisfactory mechanical properties in laboratory settings (Magne et al., 2010). Clinical studies have also confirmed the reliable performance of these composite restorations (Demarco et al., 2017; Da Rosa Rodolpho et al., 2022; Demarco et al., 2023), highlighting their potential to adhere to the biomimetic principles of conserving natural tissue (Magne et al., 2011). Nonetheless, despite recent improvements in resin composites aimed at minimizing polymerization shrinkage stress and incorporating cutting-edge fabrication techniques (Schweiger et al., 2021), these materials still present significant challenges.

In the traditional layering (incremental) technique, indirect restorations are created by applying and shaping successive thin layers of resin composite on a prepared tooth model, each cured through photopolymerization to form the final restoration shape (Klaff, 2001). However, this process can introduce bubbles that could undermine the structural integrity of the restoration (Benalcázar Jalkh et al., 2019; Nandini, 2010). Additionally, the technique demands high precision and skill from the operator to consistently achieve optimal outcomes (Shu et al., 2018; de Kuijper et al., 2023). An alternative is the use of Computer-Aided Design/Computer-Aided Manufacturing (CAD/CAM) systems, which involve digital design of the restoration using specialized software and its fabrication through precise subtractive machining with diamond drills (Digholkar et al., 2016). While this method allows for the use of various materials and offer precision, it is not without its drawbacks, including the wastage of material (Strub et al., 2006), diamond drills wear (Chen et al., 2016; Sorrentino et al., 2019), and the potential for creating surface and subsurface flaws that could lead to stress concentration and premature failure of the restoration (Blatz and Conejo, 2019).

To address these challenges, 3D printing technology has been introduced, leveraging CAD for the digital design of restorations, followed by the creation through an additive material process in a 3D printer (Jeong et al., 2018). Among the various additive manufacturing techniques, stereolithography stands out in dental applications (Lian et al., 2018). This method entails the sequential layering of a photopolymerizable resin, based on the pre-designed standard tessellation language (STL) file, which is then cured layer by layer using a laser or light-emitting diode (LED), culminating in the formation of the final 3D structure (Digholkar et al., 2016; Baroudi and Ibraheem, 2015). In addition to manufacturing advancements, efforts have been made to enhance the of 3D resins through the incorporation of additives into polymers, with the goal of improving their biological, mechanical, and aesthetic characteristics (Awada and Nathanson, 2015). Ceramic fillers, particularly zirconium oxide (ZrO_2) nanoparticles, have been recognized as highly effective additives in resin-based dental composites (Aati et al., 2021). Studies have shown that ZrO_2 nanoparticles significantly improve a range of properties, including flexural strength, fracture toughness, hardness, wear resistance, thermal stability (Gad et al., 2019; Maji et al., 2016; Reyes-Acosta et al., 2015; Ergun et al., 2018; Nakanishi et al., 2020). However, some modifications have introduced adverse effects that may ultimately impact the long-term efficacy of the materials, such as the development voids or porosity, reduced biocompatibility, limitations in curing depth, and reduced degree of C=C conversion (de Castro et al., 2017; Alhareb and Ahmad, 2011; Malic et al., 2019; Gad et al., 2019).

To date, research has predominantly concentrated on 3D printed resins for temporary restorations (Lin et al., 2020; de Castro et al., 2022; Soto-Montero et al., 2022; Aati et al., 2022; Prause et al., 2023; Finck et al., 2023). However, the advent of materials for longer-lasting printed restorations, including zirconia-containing resin composites, marks a leap forward, introducing viable options for fabricating dental crowns, veneers, inlays, and onlays. Despite their promising attributes, the endorsement of these materials for clinical applications hinges on the acquisition of comprehensive preclinical and clinical data, particularly regarding their long-term mechanical behavior (Daher et al., 2022). Fatigue tests, which mimic the degradation mechanisms of dental restorations through repetitive, low-intensity forces akin to those of chewing, are deemed crucial for evaluating the resilience of these materials (Rosentritt et al., 2016, Wendler et al., 2017).

To the best of the authors' knowledge, the fatigue resistance of 3D printed zirconia-containing resin composites remains unexplored. Thus, the aim of this study was to assess the monotonic and fatigue strength, along with the surface characteristics, of a 3D printed zirconia-containing resin, comparing it against materials with similar composition produced via subtractive and traditional layering techniques. Two null hypotheses were formulated: (1) the monotonic and fatigue flexural strengths of the 3D printed resin composite would be comparable to those fabricated by subtractive

and traditional layering techniques, and (2) the surface characteristics of the 3D printed resin composite would mirror those of composites produced by subtractive and layering techniques.

2 Material and Methods

2.1. Study design and materials tested

This in vitro study was designed to investigate the mechanical properties of zirconia-containing resin composites fabricated through three distinct methods: 3D Printing, using stereolithography; Subtractive Manufacturing; and Layering, following a conventional layering technique. A detailed summary of the materials used in this research is presented in Table 1, including commercial names, manufacturers, chemical compositions, and batch numbers. The primary outcomes assessed were the flexural strength (*FS*, in MPa) under both monotonic (n= 5) and fatigue (n= 10) loading conditions, along with the number of cycles to failure (CFF) during fatigue testing. Sample size calculation was conducted using OpenEpi (The OpenEpi Project, Atlanta, GA, USA) based on the mean and standard deviation values obtained from the monotonic *FS* tests (n= 5) for the 3D Printing (113 ±6.9) and Subtractive (161 ±38.7) groups. This analysis, which assumed an 80% power and 95% confidence level, indicated a minimum requirement of 6 discs per group. Additional evaluations included measuring the elastic modulus (*E*, in GPa), analyzing surface roughness (using Ra and Rz parameters, in μm), examining surface topography, and investigating the fractographic characteristics of the failed specimens, through scanning electron microscopy (SEM).

2.2. Specimen preparation

Specimens, both discs (n= 15; Ø= 15 mm × 1.2 mm thickness) and bars (n= 15; dimensions 14 × 4 × 1.2 mm), were fabricated in accordance with ISO 6872 (2015) standard, using the following manufacturing techniques:

3D Printing: The design process began with Tinkercad software (Autodesk, San Francisco, CA, USA) to create the digital models for the specimens. These models then converted into STL files and uploaded to a 3D printer (Phrozen Sonic Mini 4K, Hsinchu, Taiwan). The printing material used was a photopolymerizable resin (PriZma 3D Bio Crown, Makertech Labs, Tatuí, SP, Brazil), and the process followed the manufacturer's guidelines: perpendicular orientation, a layer height of 50 μm, 8 bottom layers, a linear transition type, and exposure times adjusted to 5 ± 0.5 s for regular layers and 80 s for the bottom layers. After printing, the specimens were cleaned with isopropyl alcohol for 5 min under agitation to eliminate any residual surface resin and then air-dried. The final step involved a 60 min post-curing phase in a UV light chamber (Wash & Cure Plus 3.0, Anycubic, Shenzhen, China).

Subtractive Manufacturing: The subtractive specimens were crafted from CAD/CAM zirconia-containing resin composite blocks (Lava Ultimate, 3M, Maplewood, MN, USA) measuring 13 × 15 × 18 mm. These blocks were cut using a diamond disc on a cutting machine with water cooling (ISOMET 1000, Buehler, Lake Bluff, IL, USA). During cutting, the precision machine was programmed to cut the bars and discs with an additional 0.5 mm beyond the desired dimensions to allow for polishing and surface regularization. These dimensions were verified after cutting using a digital micrometer (Absolute 500-196-20, Mitutoyo). To create discs, the blocks were first transformed into cylinders (Ø= 15) by using a series of grinding processes with SiC papers of #400, #600, and #1200 grits on a polishing machine (EcoMet/AutoMet 250, Buehler), also under water cooling. Metal guides were affixed to the blocks to ensure precision during the grinding process.

Layering: The layering specimens were initiated using a 3D printed model to create a condensation silicone guide. The guide was then cleaned with isopropyl alcohol. Following this, between 8 and 10 increments of zirconia-containing resin composite for direct restorations (Filtek Z350 XT, 3M, Maplewood, MN, USA) was applied in layers less than 2 mm thick, with each increment photopolymerized for 20 s using a LED light-curing unit (Radii-cal, SDI, Bayswater, Victoria, Australia) with intensity of 1200 mW/cm^2. A glass plate was placed over the specimen before curing the final layer to ensure a uniform surface.

To standardize the surface topography across all groups, both sides of each specimen were polished using a sequence of SiC papers of #600, #1200, and #2500 grits under water cooling. This step aimed to eliminate any surface irregularities and achieve the desired final dimensions. Additionally, the specimens were measured at 3 points (bars: center, 1/3, and 2/3) and at 4 points (discs: center and 3 regions at the edges forming a triangle) using a digital micrometer (Absolute 500-196-20, Mitutoyo). To minimize stress concentrations in the bars, chamfers were carefully added by two experienced operators (L.F.B.S. and A.C.C.R.) after a series of preliminary tests. The chamfering, ranging between 0.09 mm and 0.15 mm, was done by lightly grinding the bar edges for 5 s with #1200 grit SiC paper, as per ISO 6872 (2015) standard. The accuracy of each chamfer was verified under a stereomicroscope at 50× magnification (Discovery V20, Carl Zeiss, Gottingen, LS, Germany), and any specimens not meeting the criteria were replaced. This polishing process was conducted 24 h post-preparation of the specimens. During this period, and prior to testing, all specimens were stored in distilled water at 37 ºC for 24 h and up to a maximum of 3 days.

2.3. Surface roughness

A micrometric roughness analysis was carried out on the discs (n= 10) using a contact stylus profilometer (Mitutoyo SJ-410, Kanagawa, Japan). Six measurements were taken for each specimen, three along the *x*-axis and three along the *y*-axis, with a cut-off (λc) of 0.8 mm and a sampling length

of 4 mm. The arithmetic mean of the roughness was calculated for each specimen in accordance with ISO 21920-2 (2021), taking into account the average surface roughness (Ra) and maximum peak-to-valley height (Rz) parameters.

2.4. Monotonic and fatigue flexural strength

Five discs were subjected to a monotonic test using a biaxial flexural strength approach. This test utilized a piston-on-three-balls setup, according to ISO 6872 (2015) standard, using a universal testing machine (DL-1000 Emic, Instron, São José dos Pinhais, PR, Brazil). The specimens were placed on three steel spheres (2.5 mm in diameter, arranged 120° apart to form a 10 mm diameter circle) immersed in distilled water. To minimize contact stress concentration and prevent surface damage, a layer of cellophane tape (15 μm) was placed between the specimen and the spheres (Wachtman et al., 1972). Additionally, an adhesive tape (110 μm) was applied to the top surface of the specimen to prevent fragment scattering. A load was then applied at the disc's center at a rate of 1 mm/min using a flat-tipped circular cylinder steel piston (Ø= 1.4 mm). Maximum fracture stress (in MPa) was calculated using the following equation:

$$\sigma_{BI} = \frac{-0.2837P(X-Y)}{b^2} \quad \text{(Equation 1)},$$

where σ_{BI} represents the peak center tensile stress in MPa, P denotes the total load at fracture in N, and b is the specimen thickness in mm. The coefficients X and Y were derived from Equations 2 and 3:

$$X = (1 + \nu)\, ln\, ln\left(\frac{r2}{r3}\right) + \left(\frac{1-\nu}{2}\right)\left(\frac{r2}{r3}\right) \quad \text{(Equation 2)},$$

$$Y = (1 + \nu)\left[1 + ln\left(\frac{r1}{r3}\right)\right] + (1 - \nu)\left(\frac{r1}{r3}\right) \quad \text{(Equation 3)},$$

where ν is Poisson's ratio, and $r1$, $r2$, and $r3$ are the radii (in mm) of the support circle, piston, specimen, respectively. The monotonic *FS* in MPa was then recorded.

For the cyclic fatigue test (n= 10), a mechanical testing machine (Instron Corporation; Norwood, MA, USA) was used, maintaining the same setup of the monotonic test and using the lowest mean *FS* (3D printing) as a parameter. The initial stress level was set at approximately 20% (20 MPa), with 5% (5 MPa) stress increments at a 10 Hz frequency every 5,000 cycles up to 100 MPa, followed by 10 MPa increments until fracture. Both fatigue *FS* (in MPa) and the CFF were then noted.

2.5. Elastic modulus

The bars (n= 15) were tested for their *E* using a three-point bending monotonic test (ISO 6872, 2015) using a universal testing machine (EMIC DL 2000, São José dos Pinhais, PR, Brazil). During the test, each specimen was placed on a jig with support rollers (Ø= 2.0 mm) spaced 12 mm apart. A third roller (Ø= 2.0 mm) applied the load at a crosshead speed of 1 mm/min at bar's midpoint until fracture. To prevent fragment dispersion and minimize contact surface damage, adhesive tape (110 μm) was affixed to the top of the specimen, and additional tape was used between the specimen and the support rollers to lessen contact stress concentration (Wachtman et al., 1972). The E was calculated in GPa as follows:

$$E = \frac{PL^3}{4vbh^3} \quad \text{(Equation 4),}$$

where P represents the fracture load in N, L the test span in mm, b the width of the specimen in mm, h the thickness of the specimen in mm, and v the corresponding displacement. The ratio P / v is the slope of the load–displacement curve within the linear elastic region before deviating from linearity (López-Suevos and Dickens, 2008).

2.6. Complementary analysis

After the fatigue testing, all fractured specimens were first examined with a stereomicroscope to select representative failures from each group for further analysis. The selected specimens were then prepared for the fractographic examination using SEM (Vega3, Tescan, Brno, Czech Republic) at magnifications of 21×, 180×, and 500×, aiming to identify fractographic characteristics present. The preparation process involved cleaning the specimens in an ultrasonic cleaner (1440 D Odontobras, Ribeirão Preto, SP, Brazil) with 92% isopropyl alcohol for 5 min. Subsequently, the specimens were coated with a layer of gold-palladium alloy. In addition, to examine the surface topography, new specimens were created for each group (n= 1) and analyzed using SEM at higher magnifications of 200×, 1,000×, and 5,000×. These specimens also underwent the same cleaning process with 92% isopropyl alcohol in an ultrasonic cleaner, followed by gold-palladium alloy coating. This approach allowed for a detailed examination of both the fractographic and topographical characteristics of the specimens post-fatigue testing.

2.7. Data analysis

The data for monotonic *FS*, *E*, and surface roughness were subjected to the Shapiro-Wilk test ($p > 0.05$). The monotonic *FS* and roughness data, which showed parametric and homoscedastic distributions, were analyzed using One-way Analysis of Variance (ANOVA) and Tukey's post-hoc

tests (α= 0.05) using SPSS v. 21 software (IBM Analytics, New York, NY, USA). Conversely, the *E* data, which exhibited a non-parametric distribution (p< 0.05), were analyzed using the Kruskal-Wallis and multiple comparisons post-hoc tests (α= 0.05). For the fatigue *FS* and CFF data, Kaplan-Meier and Mantel-Cox (Log-Rank) tests were used (α= 0.05). Furthermore, the fatigue *FS* data were subjected to Weibull statistical analysis to evaluate the material's characteristic strength and reliability, using the SuperSMITH Weibull 4.0k-32 software (Wes Fulton, Torrance, CA, USA). Statistical differences were discerned through maximum-likelihood estimation by examining the overlap of confidence intervals, where a lack of overlap indicated differences in such parameters. In addition, fractographic and topographic features were qualitatively analyzed to identify the origins of failure and the surface topographic patterns of the resin composite specimens.

3 Results

In the monotonic tests (Table 2), the Subtractive group exhibited higher *FS* when compared to both the 3D Printing (p= 0.02) and Layering (p= 0.04) groups, while the 3D Printing and Layering methods yielded similar *FS* results (p= 0.88). The fatigue tests (Tables 2 and 3) revealed distinct statistical differences among all groups in terms of *FS* and CFF, with the ranking from lowest to highest being 3D printing, Layering, and Subtractive (p< 0.01 and p= 0.04, respectively). The Weibull analysis showed similar characteristic strength between Subtractive and Layering, which were superior to 3D printing. Weibull modulus, reflecting mechanical reliability, showed no significant differences among the groups (Table 2).

As shown in Figure 1, comparisons of *E* across the manufacturing techniques revealed no significant differences between the 3D Printing and Subtractive methods (p= 0.24), both of which exhibited higher *E* than the Layering technique (3D Printing vs. Layering: p< 0.01; Subtractive vs. Layering: p= 0.01). Surface roughness analysis (Figure 2) indicated that the 3D Printing group had significantly rougher surfaces than both Subtractive (Ra: p< 0.01; Rz: p< 0.01) and Layering (Ra: p< 0.01; Rz: p= 0.04) groups, while Subtractive and Layering showed comparable roughness (Ra: p= 0.19; Rz: p= 0.06).

Fractographic analysis (Figure 3) indicated that fractures typically originated from surface defects located in the areas subjected to tensile stress concentration. SEM images (Figure 4) highlighted an irregular and porous surface in the 3D Printing group, in contrast to the more uniform surfaces with visible filler particles in both the Subtractive and Layering groups, though minor surface defects were also present in these groups.

4 Discussion

The findings from this study indicated a superior monotonic strength in the Subtractive group when compared to both the 3D Printing and Layering groups, with the latter showing comparable results to one another. In terms of fatigue strength, the Subtractive group outperformed the Layering group, which in turn exceeded the performance of the 3D Printing group. The characteristic strength showed that Subtractive and Layering were similar, but both superior to 3D printing, although the Weibull modulus remained similar for all groups. These observations led to the rejection of the first null hypothesis proposed in this study. Additionally, the 3D Printing group was found to have a higher surface roughness than both the Subtractive and Layering groups, resulting in the rejection of the second null hypothesis as well.

The manner in which materials are processed plays a pivotal role in the formation of surface flaws, particularly in 3D printed materials (Kessler et al., 2021; Bergamo et al., 2022; Atria et al., 2022). Previous studies have shown that the presence and concentration of filler particles can obstruct the flow of the resin the building process, leading to an increased likelihood of air bubble entrapment and a subsequent decline in mechanical properties (De Castro et al., 2022). Additionally, the extent of monomer conversion into the polymer network is a critical factor affecting mechanical properties, with higher conversion rates leading to improved material characteristics (Ferracane, 1985). The degree of C=C conversion in resin composites is significantly influenced by various factors including the irradiance and wavelength of the light curing, exposure duration, material translucency, and the scattering of light by filler particles (Halvorson et al., 2002; Leloup et al., 2002). It has been reported in recent research (Aati et al., 2021) that the incorporation of nano-ZrO_2 into 3D printed resin can markedly reduce the degree of conversion, attributed to the opaque nature of ZrO_2 fillers, which impedes effective light dispersion. In line with these observations, the 3D printed specimens exhibited rougher surfaces, a finding corroborated by SEM imaging (Figure 4). The images showed the presence of voids in the 3D printed resin composite, likely resulting from the uneven mixing of resin components and constraints encountered during the polymerization process.

Despite the printed resin showing comparable monotonic strength to the conventionally layered resin, this similarity could be due to the higher *E* observed in the printed resin. This increased stiffness suggests that such materials possess greater resistance to deformation before fracturing (Perea-Lowery et al., 2020). However, during the fatigue tests, which emphasize the impact of defects under cyclic loading, the defects in the printed resin seemed to play a significant role, leading to the conventional layering technique's relative superiority. Similarly, inherent defects associated with the conventional layering process (Ibrahim et al., 2023) might have been a decisive factor in its reduced fatigue strength compared to the subtractive method, as both techniques exhibited similar roughness, topography, and material composition.

The biaxial *FS* and characteristic strength findings were consistent with previous studies, which reported similar *FS* (Lin et al., 2020; de Castro et al., 2022; Soto-Montero et al., 2022; Aati et al., 2022; Prause et al., 2023) or slightly lower *FS* (Scotti et al., 2020; Bergamo et al., 2022; de Castro et al., 2022) for 3D printed resin composites. In contrast, certain studies have indicated higher strength values compared to those observed in the current study (Grzebieluch et al., 2021; Bayarsaikhan et al., 2022; Atria et al., 2022; Taşın and Ismatullaev, 2022). The variation in results could be due to differences in experimental setups for measuring *FS*, the specific types of 3D printing materials tested, and the printing techniques used. Additionally, testing under humid conditions that foster hydrolytic effects might have contributed to the reduced strength of the 3D printed resin composite examined in our study.

It is essential to acknowledge that despite the variations observed in monotonic and fatigue strengths, the materials satisfied the ISO 6872 (2015) standards for Class 2 category, which requires a *FS* greater than 100 MPa for clinical applications in adhesively luted anterior or posterior single-unit monolithic prostheses. The printed material was the only one to show a marginal shortfall in terms of fatigue performance, with its strength dipping below the 100 MPa benchmark, suggesting the necessity for material optimization concerning mechanical properties. In this context, as mentioned earlier, the mixing process of the components of the 3D printed resin composite under investigation, along with the fabrication method, needs refinement to achieve a more uniform distribution of constituents, thereby ensuring superior mechanical properties (Kessler et al., 2019; Prause et al., 2022).

Regarding the results of surface roughness, beyond their impact on mechanical properties, where a smoother surface is often associated with greater strength than a rough one (Ramezanzadeh et al., 2010), it is important to emphasize that the higher roughness observed in the printed resin may lead to a compromised restoration aesthetics, including surface staining and reduced gloss. Furthermore, there is clear evidence of the association between roughness and biofilm adhesion and maturation (Brambilla et al., 2005; Ono et al., 2007; McConnell et al., 2010), which can cause other complications such as gingival inflammation, secondary caries, and bacterial plaque accumulation (Panyayong et al., 2002). However, it’s noteworthy that the Ra value for the 3D printing group remained below the critical threshold of 0.2 μm, which is considered significant for microbial plaque accumulation (Bollen et al., 1997; Dutra et al., 2018).

While this study has certain limitations, it also presents novel insights and contributions to the field. The use of CAD/CAM blocks with dimensions of 13 × 15 × 18 mm, although not fully aligned with ISO 4049 (2019) minimum dimension recommendations of 25 × 2 × 2 mm, was necessary within the context of our research. The testing methodology, while traditionally employed for ceramics as per ISO 6872 (2015), was adapted to suit our study's specific focus on comparing the 3D printed

zirconia-containing composite with a subtractive technique. In addition, the study did not replicate the geometric complexities of bonded restorations or explore the effects of bonding the resin composites to supporting dental substrates, for instance. Furthermore, it is important to recognize the lack of correction for the deformation introduced by the soft tape in elastic modulus evaluation, although this limitation equally affected all groups within our study. Therefore, while the results may be influenced by the presence of the tape, internal comparisons between the groups can still be valid within the context of this study. Despite these considerations, this research stands out as potentially the first to explore the fatigue mechanical properties of 3D printed zirconia-containing resin composites. A significant advantage of this study is the use of cyclic testing in aqueous environments to assess bending, providing a simple yet effective approach to understanding the mechanical degradation of indirect materials due to cyclic loading and crack progression (Zhang et al., 2023). We anticipate that our findings will pave the way for further laboratory studies, including those with bonded restorations and various types of 3D printed resins, to enhance the understanding about the potential durability of 3D-printed restoratives.

5 Conclusion

Based on the results obtained for the materials of this study, it is possible to distinguish the unique properties of 3D printed resin composite when contrasted with established techniques like conventional layering and subtractive methods for resin-based materials. The following conclusions can be drawn:

1. 3D printed resin exhibited monotonic strength comparable to that of conventional layering;
2. Subtractive resin demonstrated superior fatigue strength relative to both conventional layering and 3D printed resin, with conventional layering outperforming 3D printing in this aspect;
3. Subtractive and layering resin showed similar characteristic strength, being superior to 3D printed resin;
4. Both 3D printed and subtractive resin presented similar elastic moduli, exceeding that of the conventional layering technique;
5. The 3D printed resin had a higher surface roughness than both the subtractive and conventional layering techniques;

Declaration of competing interest

The authors declare the absence of any conflicts of interest.

Acknowledgements

This study is part of the fulfillment of the requirements of the L.F.B.S.'s PhD degree in the Faculty of Dentistry, Federal University of Santa Maria (Rio Grande do Sul State, Brazil). This research was funded by the Brazilian National Council for Scientific and Technological Development (CNPq) (L.F.B.S. doctorate scholarships, #162322/2022-4, G.K.R.P. research grant, #304665/2022-3, L.F.V CNPq Universal Call 2024-27, # 405171/2023-4), by the Brazilian Federal Agency for Coordination of Improvement of Higher Education Personnel (CAPES) (K.F.T. Doctorate's scholarship; Finance Code 001), and by the Financial Agency for Studies and Projects (FINEP) (Rapid Prototyping, Additive Manufacturing, Innovation and Services Laboratory (Lab3D+), #0123006500). We emphasize that those institutions had no role in the study design, data collection or analysis, decision to publish, or manuscript preparation.

REFERENCES

1. Aati, S., Akram, Z., Ngo, H., & Fawzy, A. S. (2021). Development of 3D printed resin reinforced with modified ZrO2 nanoparticles for long-term provisional dental restorations. Dental material: official publication of the Academy of Dental Materials, 37(6), e360–e374. https://doi.org/10.1016/j.dental.2021.02.010
2. Aati, S., Chauhan, A., Shrestha, B., Rajan, S. M., Aati, H., & Fawzy, A. (2022). Development of 3D printed dental resin nanocomposite with graphene nanoplatelets enhanced mechanical properties and induced drug-free antimicrobial activity. Dental materials: official publication of the Academy of Dental Materials, 38(12), 1921–1933. https://doi.org/10.1016/j.dental.2022.10.001
3. Alhareb A.O., Ahmad Z.A. (2011). Effect of Al2O3/ZrO2 reinforcementon the mechanical properties of PMMA denture base. Journal of Reinforced Plastics and Composites, 30, 86–93. https://doi.org/10.1177/0731684410379511
4. Atria, P. J., Bordin, D., Marti, F., Nayak, V. V., Conejo, J., Benalcázar Jalkh, E., Witek, L., & Sampaio, C. S. (2022). 3D-printed resins for provisional dental restorations: Comparison of mechanical and biological properties. Journal of esthetic and restorative dentistry: official publication of the American Academy of Esthetic Dentistry, 34(5), 804–815. https://doi.org/10.1111/jerd.12888
5. Awada, A., & Nathanson, D. (2015). Mechanical properties of resin-ceramic CAD/CAM restorative materials. The Journal of prosthetic dentistry, 114(4), 587–593. https://doi.org/10.1016/j.prosdent.2015.04.016
6. Baroudi, K., & Ibraheem, S. N. (2015). Assessment of Chair-side Computer-Aided Design and Computer-Aided Manufacturing Restorations: A Review of the Literature. Journal of international oral health: JIOH, 7(4), 96–104.
7. Bayarsaikhan, E., Gu, H., Hwangbo, N. K., Lim, J. H., Shim, J. S., Lee, K. W., & Kim, J. E. (2022). Influence of different postcuring parameters on mechanical properties and biocompatibility of 3D printed crown and bridge resin for temporary restorations. Journal of the mechanical behavior of biomedical materials, 128, 105127. https://doi.org/10.1016/j.jmbbm.2022.105127
8. Benalcázar Jalkh, E. B., Machado, C. M., Gianinni, M., Beltramini, I., Piza, M., Coelho, P. G., Hirata, R., & Bonfante, E. A. (2019). Effect of Thermocycling on Biaxial Flexural Strength of CAD/CAM, Bulk Fill, and Conventional Resin Composite Materials. Operative dentistry, 44(5), E254–E262. https://doi.org/10.2341/18-146-L
9. Bergamo, E. T. P., Campos, T. M. B., Piza, M. M. T., Gutierrez, E., Lopes, A. C. O., Witek, L., Coelho, P. G., Celestrino, M., Carvalho, L. F., Benalcázar Jalkh, E. B., & Bonfante, E. A. (2022).

Temporary materials used in prosthodontics: The effect of composition, fabrication mode, and aging on mechanical properties. Journal of the mechanical behavior of biomedical materials, 133, 105333. https://doi.org/10.1016/j.jmbbm.2022.105333

10. Blatz, M. B., & Conejo, J. (2019). The Current State of Chairside Digital Dentistry and Materials. Dental clinics of North America, 63(2), 175–197. https://doi.org/10.1016/j.cden.2018.11.002
11. Bollen, C. M., Lambrechts, P., & Quirynen, M. (1997). Comparison of surface roughness of oral hard materials to the threshold surface roughness for bacterial plaque retention: a review of the literature. Dental materials: official publication of the Academy of Dental Materials, 13(4), 258–269. https://doi.org/10.1016/s0109-5641(97)80038-3
12. Brambilla, E., Cagetti, M.G., Gagliani, M., Fadini, L., García-Godoy, F., Strohmenger, L., 2005. Influence of different adhesive restorative materials on mutans streptococci colonization. Am. J. Dent. 18, 173–176.
13. Chen, Y. W., Moussi, J., Drury, J. L., & Wataha, J. C. (2016). Zirconia in biomedical applications. Expert review of medical devices, 13(10), 945–963. https://doi.org/10.1080/17434440.2016.1230017
14. Da Rosa Rodolpho, P. A., Rodolfo, B., Collares, K., Correa, M. B., Demarco, F. F., Opdam, N. J. M., Cenci, M. S., & Moraes, R. R. (2022). Clinical performance of posterior resin composite restorations after up to 33 years. Dental materials: official publication of the Academy of Dental Materials, 38(4), 680–688. https://doi.org/10.1016/j.dental.2022.02.009
15. Daher, R., Ardu, S., di Bella, E., Krejci, I., & Duc, O. (2022). Efficiency of 3D-printed composite resin restorations compared with subtractive materials: Evaluation of fatigue behavior, cost, and time of production. The Journal of prosthetic dentistry, S0022-3913(22)00481-4. Advance online publication. https://doi.org/10.1016/j.prosdent.2022.08.001
16. de Castro, D. T., Valente, M. L. D. C., Aires, C. P., Alves, O. L., & Dos Reis, A. C. (2017). Elemental ion release and cytotoxicity of antimicrobial acrylic resins incorporated with nanomaterial. Gerodontology, 34(3), 320–325. https://doi.org/10.1111/ger.12267
17. de Castro, E. F., Nima, G., Rueggeberg, F. A., & Giannini, M. (2022). Effect of build orientation in accuracy, flexural modulus, flexural strength, and microhardness of 3D-Printed resins for provisional restorations. Journal of the mechanical behavior of biomedical materials, 136, 105479. https://doi.org/10.1016/j.jmbbm.2022.105479
18. de Kuijper, M. C. F. M., Cune, M. S., Özcan, M., & Gresnigt, M. M. M. (2023). Clinical performance of direct composite resin versus indirect restorations on endodontically treated posterior teeth: A systematic review and meta-analysis. The Journal of prosthetic dentistry, 130(3), 295–306. https://doi.org/10.1016/j.prosdent.2021.11.009

19. Demarco, F. F., Collares, K., Correa, M. B., Cenci, M. S., Moraes, R. R., & Opdam, N. J. (2017). Should my composite restorations last forever? Why are they failing?. Brazilian oral research, 31(suppl 1), e56. https://doi.org/10.1590/1807-3107BOR-2017.vol31.0056
20. Demarco, F. F., Cenci, M. S., Montagner, A. F., de Lima, V. P., Correa, M. B., Moraes, R. R., & Opdam, N. J. M. (2023). Longevity of composite restorations is definitely not only about materials. Dental materials: official publication of the Academy of Dental Materials, 39(1), 1–12. https://doi.org/10.1016/j.dental.2022.11.009
21. Digholkar, S., Madhav, V. N., & Palaskar, J. (2016). Evaluation of the flexural strength and microhardness of provisional crown and bridge materials fabricated by different methods. Journal of Indian Prosthodontic Society, 16(4), 328–334. https://doi.org/10.4103/0972-4052.191288
22. Dutra, D., Pereira, G., Kantorski, K. Z., Valandro, L. F., & Zanatta, F. B. (2018). Does Finishing and Polishing of Restorative Materials Affect Bacterial Adhesion and Biofilm Formation? A Systematic Review. Operative dentistry, 43(1), E37–E52. https://doi.org/10.2341/17-073-L
23. Edelhoff, D., Erdelt, K. J., Stawarczyk, B., & Liebermann, A. (2023). Pressable lithium disilicate ceramic versus CAD/CAM resin composite restorations in patients with moderate to severe tooth wear: Clinical observations up to 13 years. Journal of esthetic and restorative dentistry: official publication of the American Academy of Esthetic Dentistry, 35(1), 116–128. https://doi.org/10.1111/jerd.12947
24. Ergun, G., Sahin, Z., & Ataol, A. S. (2018). The effects of adding various ratios of zirconium oxide nanoparticles to poly(methyl methacrylate) on physical and mechanical properties. Journal of oral science, 60(2), 304–315. https://doi.org/10.2334/josnusd.17-0206
25. Ferracane J. L. (1985). Correlation between hardness and degree of conversion during the setting reaction of unfilled dental restorative resins. Dental materials: official publication of the Academy of Dental Materials, 1(1), 11–14. https://doi.org/10.1016/S0109-5641(85)80058-0
26. Finck, N. S., Fraga, M. A. A., Correr, A. B., Dalmaschio, C. J., Rodrigues, C. S., & Moraes, R. R. (2023). Effects of solvent type and UV post-cure time on 3D-printed restorative polymers. Dental materials: official publication of the Academy of Dental Materials, S0109-5641(23)00487-6. Advance online publication. https://doi.org/10.1016/j.dental.2023.12.005
27. Gad, M. M., Al-Thobity, A. M., Rahoma, A., Abualsaud, R., Al-Harbi, F. A., & Akhtar, S. (2019). Reinforcement of PMMA Denture Base Material with a Mixture of ZrO2 Nanoparticles and Glass Fibers. International journal of dentistry, 2489393. https://doi.org/10.1155/2019/2489393
28. Grzebieluch, W., Kowalewski, P., Grygier, D., Rutkowska-Gorczyca, M., Kozakiewicz, M., & Jurczyszyn, K. (2021). Printable and Machinable Dental Restorative Composites for CAD/CAM

Application-Comparison of Mechanical Properties, Fractographic, Texture and Fractal Dimension Analysis. Materials (Basel, Switzerland), 14(17), 4919. https://doi.org/10.3390/ma14174919

29. Halvorson, R. H., Erickson, R. L., & Davidson, C. L. (2002). Energy dependent polymerization of resin-based composite. Dental materials: official publication of the Academy of Dental Materials, 18(6), 463–469. https://doi.org/10.1016/s0109-5641(01)00069-0
30. ISO 21920-2, 2021. Geometrical Product Specifications (GPS) - Surface texture: Profile Part 2: Terms, definitions and surface texture parameters. International Organization for Standardization, Geneva, Switzerland.
31. ISO 4049, 2019. Dentistry: Polymer-based restorative materials. International Organization for Standardization, Geneva, Switzerland.
32. ISO 6872, 2015. Dentistry - Ceramic Materials. International Organization for Standardization, Geneva, Switzerland.
33. Jeong, Y. G., Lee, W. S., & Lee, K. B. (2018). Accuracy evaluation of dental models manufactured by CAD/CAM milling method and 3D printing method. The journal of advanced prosthodontics, 10(3), 245–251. https://doi.org/10.4047/jap.2018.10.3.245
34. Keßler, A., Hickel, R., & Ilie, N. (2021). In vitro investigation of the influence of printing direction on the flexural strength, flexural modulus and fractographic analysis of 3D-printed temporary materials. Dental materials journal, 40(3), 641–649. https://doi.org/10.4012/dmj.2020-147
35. Kessler, A., Reymus, M., Hickel, R., & Kunzelmann, K. H. (2019). Three-body wear of 3D printed temporary materials. Dental materials: official publication of the Academy of Dental Materials, 35(12), 1805–1812. https://doi.org/10.1016/j.dental.2019.10.005
36. Klaff D. (2001). Blending incremental and stratified layering techniques to produce an esthetic posterior composite resin restoration with a predictable prognosis. Journal of esthetic and restorative dentistry: official publication of the American Academy of Esthetic Dentistry, 13(2), 101–113. https://doi.org/10.1111/j.1708-8240.2001.tb00432.x
37. Kunzelmann, K. H., Jelen, B., Mehl, A., & Hickel, R. (2001). Wear evaluation of MZ100 compared to ceramic CAD/CAM materials. International journal of computerized dentistry, 4(3), 171–184.
38. Leloup, G., Holvoet, P. E., Bebelman, S., & Devaux, J. (2002). Raman scattering determination of the depth of cure of light-activated composites: influence of different clinically relevant parameters. Journal of oral rehabilitation, 29(6), 510–515. https://doi.org/10.1046/j.1365-2842.2002.00889.x

39. Lian, Q.; Sui, W.; Wu, X.; Yang, F.; Yang, S. (2018). Additive manufacturing of Zr02 ceramic dental bridges by stereolithography. Rapid Prototyping Journal, 24(1), 114–119.
40. Lin, C. H., Lin, Y. M., Lai, Y. L., & Lee, S. Y. (2020). Mechanical properties, accuracy, and cytotoxicity of UV-polymerized 3D printing resins composed of Bis-EMA, UDMA, and TEGDMA. The Journal of prosthetic dentistry, 123(2), 349–354. https://doi.org/10.1016/j.prosdent.2019.05.002
41. Magne, P., Paranhos, M. P., & Schlichting, L. H. (2011). Influence of material selection on the risk of inlay fracture during pre-cementation functional occlusal tapping. Dental materials: official publication of the Academy of Dental Materials, 27(2), 109–113. https://doi.org/10.1016/j.dental.2010.09.002
42. Magne, P., Perakis, N., Belser, U. C., & Krejci, I. (2002). Stress distribution of inlay-anchored adhesive fixed partial dentures: a finite element analysis of the influence of restorative materials and abutment preparation design. The Journal of prosthetic dentistry, 87(5), 516–527. https://doi.org/10.1067/mpr.2002.124367.
43. Magne, P., Schlichting, L. H., Maia, H. P., & Baratieri, L. N. (2010). In vitro fatigue resistance of CAD/CAM composite resin and ceramic posterior occlusal veneers. The Journal of prosthetic dentistry, 104(3), 149–157. https://doi.org/10.1016/S0022-3913(10)60111-4
44. Maji P., Choudhary R.B., Majhi M. (2016). Structural, optical and dielectric properties of ZrO2 reinforced polymeric nanocomposite films of polymethylmethacrylate (PMMA). Optik, 127, 4848–53. https://doi.org/10.1016/j.ijleo.2016.02.025
45. Malic, S., Rai, S., Redfern, J., Pritchett, J., Liauw, C. M., Verran, J., & Tosheva, L. (2019). Zeolite-embedded silver extends antimicrobial activity of dental acrylics. Colloids and surfaces. B, Biointerfaces, 173, 52–57. https://doi.org/10.1016/j.colsurfb.2018.09.043
46. McConnell, M.D., Liu, Y., Nowak, A.P., Pilch, S., Masters, J.G., Composto, R.J., 2010. Bacterial plaque retention on oral hard materials: Effect of surface roughness, surface composition, and physisorbed polycarboxylate. J. Biomed. Mater. Res. - Part A 92, 1518–1527. https://doi.org/10.1002/jbm.a.32493
47. Nakanishi, L., Kaizer, M. R., Brandeburski, S., Cava, S. S., Della Bona, A., Zhang, Y., & Moraes, R. R. (2020). Non-silicate nanoparticles for improved nanohybrid resin composites. Dental materials: official publication of the Academy of Dental Materials, 36(10), 1314–1321. https://doi.org/10.1016/j.dental.2020.07.001
48. Nandini S. (2010). Indirect resin composites. Journal of conservative dentistry: JCD, 13(4), 184–194. https://doi.org/10.4103/0972-0707.73377

49. Ono, M., Nikaido, T., Iked, M., Imai, S., Hanada, N., Tagami, J., Matin, K., 2007. Surface properties of resin composite materials relative to biofilm formation. Dent. Mater. J. 26, 613–622. https://doi.org/10.4012/dmj.26.613
50. Panyayong, W., Oshida, Y., Andres, C. J., Barco, T. M., Brown, D. T., & Hovijitra, S. (2002). Reinforcement of acrylic resins for provisional fixed restorations. Part III: effects of addition of titania and zirconia mixtures on some mechanical and physical properties. Bio-medical materials and engineering, 12(4), 353–366.
51. Prause E., Hey J., Beuer F., Schmidt F. (2022). Wear resistance of 3D-printed materials: a systematic review. Dentistry Review, 2(2), 100051. https://doi.org/10.1016/j.dentre.2022.100051
52. Ramezanzadeh B., Attar M.M., Farzam M. (2010). Effect of ZnO nanoparticles on the thermal and mechanical properties of epoxy-based nanocomposite. Journal of Thermal Analysis and Calorimetry, 103, 731–739. https://doi.org/10.1007/s10973-010-0996-1
53. Reyes-Acosta M.A., Torres-Huerta A.M., Dominguez-Crespo M.A., Flores-Vela A.I., Dorantes-Rosales H.J., Ramírez-Meneses E. (2015) Influence of ZrO2nanoparticles and thermal treatment on the properties of PMMA/ZrO2 hybrid coatings. Journal of Alloys and Compounds, 643, 150–158. https://doi.org/10.1016/j.jallcom.2014.10.040
54. Rosentritt, M., Behr, M. & Preis, V. A Critical Evaluation of Fatigue Studies for Restorative Materials in Dentistry. Curr Oral Health Rep 3, 221–228 (2016). https://doi.org/10.1007/s40496-016-0097-8
55. Schlichting, L. H., Resende, T. H., Reis, K. R., Raybolt Dos Santos, A., Correa, I. C., & Magne, P. (2022). Ultrathin CAD-CAM glass-ceramic and composite resin occlusal veneers for the treatment of severe dental erosion: An up to 3-year randomized clinical trial. The Journal of prosthetic dentistry, 128(2), 158.e1–158.e12. https://doi.org/10.1016/j.prosdent.2022.02.009
56. Schweiger, J., Edelhoff, D., & Güth, J. F. (2021). 3D Printing in Digital Prosthetic Dentistry: An Overview of Recent Developments in Additive Manufacturing. Journal of clinical medicine, 10(9), 2010. https://doi.org/10.3390/jcm10092010
57. Scotti, C. K., Velo, M. M. A. C., Rizzante, F. A. P., Nascimento, T. R. L., Mondelli, R. F. L., & Bombonatti, J. F. S. (2020). Physical and surface properties of a 3D-printed composite resin for a digital workflow. The Journal of prosthetic dentistry, 124(5), 614.e1–614.e5. https://doi.org/10.1016/j.prosdent.2020.03.029
58. Shu, X., Mai, Q. Q., Blatz, M., Price, R., Wang, X. D., & Zhao, K. (2018). Direct and Indirect Restorations for Endodontically Treated Teeth: A Systematic Review and Meta-analysis, IAAD 2017 Consensus Conference Paper. The journal of adhesive dentistry, 20(3), 183–194. https://doi.org/10.3290/j.jad.a40762

59. Sorrentino, R., Navarra, C. O., Di Lenarda, R., Breschi, L., Zarone, F., Cadenaro, M., & Spagnuolo, G. (2019). Effects of Finish Line Design and Fatigue Cyclic Loading on Phase Transformation of Zirconia Dental Ceramics: A Qualitative Micro-Raman Spectroscopic Analysis. Materials (Basel, Switzerland), 12(6), 863. https://doi.org/10.3390/ma12060863
60. Soto-Montero, J., de Castro, E. F., Romano, B. C., Nima, G., Shimokawa, C. A. K., & Giannini, M. (2022). Color alterations, flexural strength, and microhardness of 3D printed resins for fixed provisional restoration using different post-curing times. Dental materials: official publication of the Academy of Dental Materials, 38(8), 1271–1282. https://doi.org/10.1016/j.dental.2022.06.023
61. Strub, J. R., Rekow, E. D., & Witkowski, S. (2006). Computer-aided design and fabrication of dental restorations: current systems and future possibilities. Journal of the American Dental Association (1939), 137(9), 1289–1296. https://doi.org/10.14219/jada.archive.2006.0389
62. Taşın, S., & Ismatullaev, A. (2022). Comparative evaluation of the effect of thermocycling on the mechanical properties of conventionally polymerized, CAD-CAM milled, and 3D-printed interim materials. The Journal of prosthetic dentistry, 127(1), 173.e1–173.e8. https://doi.org/10.1016/j.prosdent.2021.09.020
63. Wendler, M., Belli, R., Valladares, D., Petschelt, A., & Lohbauer, U. (2018). Chairside CAD/CAM materials. Part 3: Cyclic fatigue parameters and lifetime predictions. Dental materials: official publication of the Academy of Dental Materials, 34(6), 910–921. https://doi.org/10.1016/j.dental.2018.03.024

TABLES

Table 1. Description of materials, brands, manufacturers, chemical compositions and batch numbers

Material	Brand/manufacturer	Chemical composition	Batch number
3D printing zirconia-containing resin composite	PriZma 3D Bio Crown, MakertechLabs, Tatuí, São Paulo, Brazil	UDMA >75%; methacryl-modified monomers >10%; zirconia <2%; ceramic fillers <15%; amorphous silica <8%	256823
CAD/CAM zirconia-containing resin composite	Lava Ultimate, 3M, Maplewood, MN, USA	Organic phase: Bis-GMA, Bis-EMA, TEGDMA, UDMA; Inorganic phase: silica (20 nm) and zirconia (4–11 nm) fillers, zirconia-silica clusters (0.6–10 μm); 79 wt% loading	N895353
Conventional zirconia-containing resin composite	Filtek Z350 XT, 3M, Maplewood, MN, USA	Organic phase: Bis-GMA, UDMA, TEGDMA, Bis-EMA; Inorganic phase: silica (20 nm non-agglomerated), zirconia, 72.5 wt% loading	NE46370

*The chemical composition is described according to the manufacturers' information.

Table 2 - Mean (MPa), standard deviation (SD), 95% confidence intervals (CI), and Weibull modulus (*m*) for the monotonic and fatigue strength (FS) tests, and for number of cycles for failure (CFF) during fatigue testing

Group	Monotonic (MPa)		FS (MPa)		% decrease between Monotonic and Fatigue means	CFF (Counts)		Weibull***	
	Mean ± SD*	95% CI	Mean ± SD**	95% CI		Mean ± SD**	95% CI	*m* (95% CI)	Characteristic strength (95% CI)
3D printing	113 ± 6.9 ^{B}	104 – 122	79 ± 8.8 ^{C}	72 – 84	30.1	44,448 ± 8,906 ^{A}	38,077 – 50,818	7.3 ^{A} 4.4 – 10.6	72.5 ^{B} 65.5 – 79.7
Subtractive	161 ± 38.7 ^{A}	113 – 209	133 ± 10.6 ^{A}	125 – 141	17.4	86,969 ± 5,100 ^{AB}	83,321 – 90,617	12.4 ^{A} 7.5 – 18.3	115.1 ^{A} 108.4 – 121.7
Layering	120 ± 5.7 ^{B}	113 – 127	116 ± 20.6 ^{B}	102 – 131	3.3	77,516 ± 15,129 ^{B}	66,693 – 88,339	8.5 ^{A} 4.7 – 13.4	105.2 ^{A} 96.3 – 114.4

* Similar letters in a column indicate no statistical differences, as determined by one-way ANOVA (α= 0.05).

** Different letters in columns indicate statistical differences, as identified by Kaplan Meier and Mantel Cox post-hoc tests (α= 0.05).

*** Similar letters in a column signify no statistical differences according to Weibull analysis using the maximum likelihood estimation method, with overlapping 95% confidence intervals indicating statistical similarities.

Table 3. Survival probabilities and their respective standard error measurements considering the progression of steps during fatigue testing (strength and number of cycles for failure).

Group	Strength (MPa) / Number of cycles																			
	20/5 ×10³	**25/10 ×10³**	**30/15 ×10³**	**35/20 ×10³**	**40/25 ×10³**	**45/30 ×10³**	**50/35 ×10³**	**55/40 ×10³**	**60/45 ×10³**	**65/50 ×10³**	**70/55 ×10³**	**75/60 ×10³**	**80/65 ×10³**	**85/70 ×10³**	**90/75 ×10³**	**95/80 ×10³**	**100/85 ×10³**	**110/90 ×10³**	**120/95 ×10³**	**130/100 ×10³**	**140/105 ×10³**	**150/110 ×10³**
3D printing	1	…	…	…	…	…	…	…	…	…	0.80 (0.13)	0.40 (0.16)	0.20 (0.13)	0.10 (0.10)	…	…	0 (0)	-	-	-	-	-
Subtractive	1	…	…	…	…	…	…	…	…	…	…	…	…	…	…	…	…	…	0.80 (0.13)	0.30 (0.15)	0.20 (0.13)	0 (0)
Layering	1	…	…	…	…	…	…	…	…	…	0.90 (0.10)	…	…	…	…	0.80 (0.13)	…	0.70 (0.15)	0.40 (0.16)	0.10 (0.10)	0 (0)	-

- The symbol "-" indicates absence of specimen survival on the considered step.
- The symbol "..." indicates absence of specimen failure in the respective step.

Figures

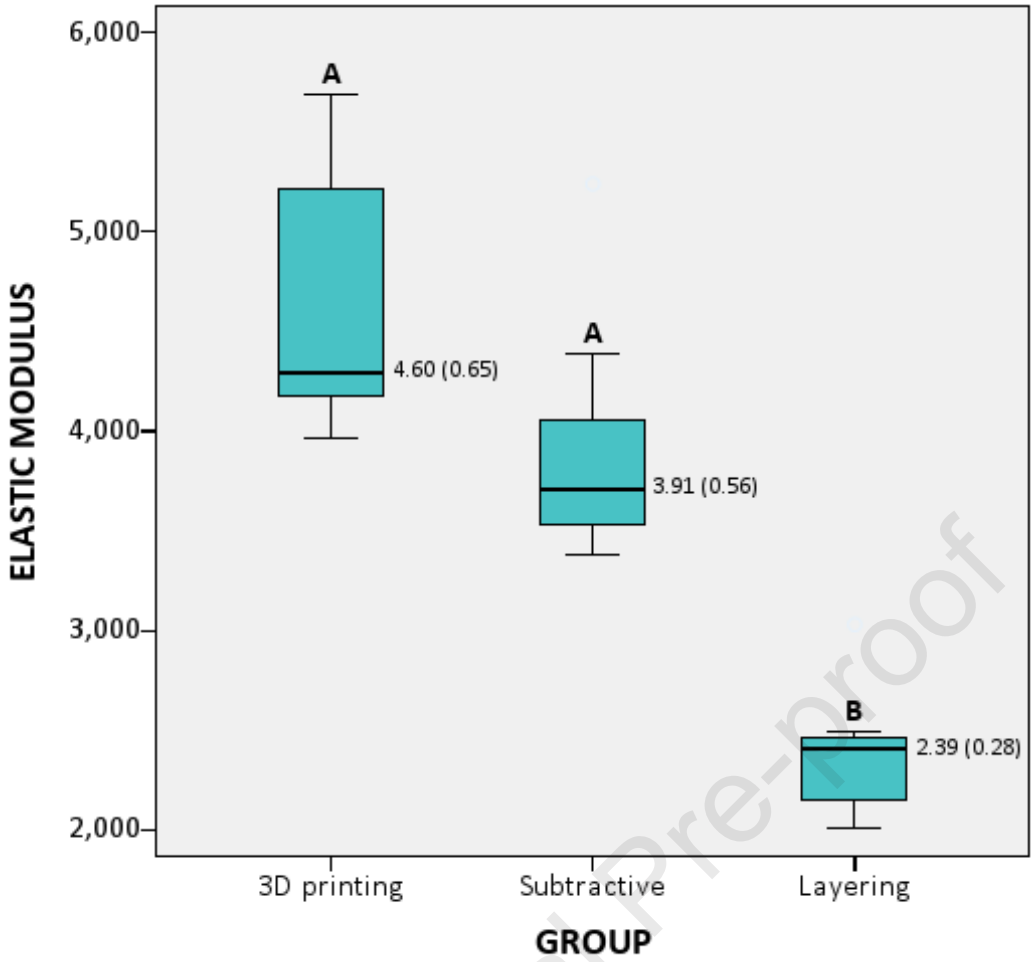

Figure 1. Box plots representing the elastic modulus (*E*, in GPa) across different groups. The box spans the interquartile range, encompassing the lower and upper quartiles (25%) of the data, with the median marked by the vertical line bisecting the box. The whiskers extend to the minimum and maximum values. The graph also includes the mean and standard deviation (SD) for *E*. Uppercase letters above each box plot indicate statistical differences among the groups, as determined by Kruskal-Wallis and multiple comparisons post-hoc tests ($\alpha = 0.05$). The 3D Printing and Subtractive methods showed comparable *E* ($p = 0.24$), and both methods exhibited higher moduli compared to the Layering method (3D Printing vs. Layering: $p < 0.01$; Subtractive vs. Layering: $p = 0.01$).

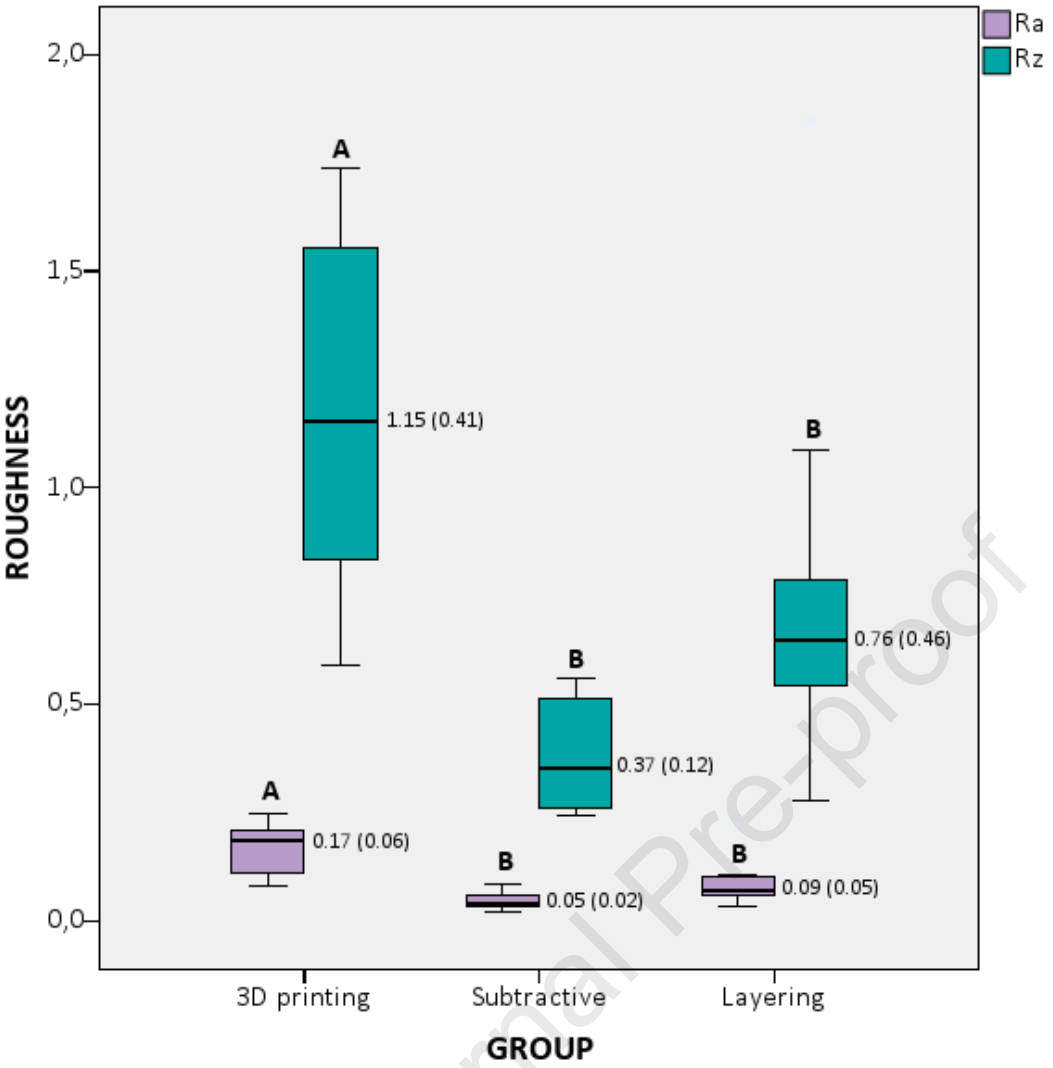

Figure 2. Box plots detailing the surface roughness parameters—Ra and Rz (in µm)—across various groups. Each box plot spans the interquartile range, capturing the lower and upper quartiles (25%) of the data, with the median depicted by the central vertical line. The whiskers extend to the minimum and maximum values observed. The graph also indicates the mean and standard deviation (SD) for both Ra and Rz. Uppercase letters above each box plot signify statistical differences in surface roughness parameters among the groups, as established by One-way ANOVA and Tukey's post-hoc tests ($\alpha = 0.05$). The 3D Printing group showed significantly higher roughness compared to both the Subtractive and Layering groups (Ra: $p < 0.01$; Rz: $p < 0.01$ for both comparisons). Meanwhile, the Subtractive and Layering groups demonstrated comparable levels of surface roughness to each other (Ra: $p = 0.19$; Rz: $p = 0.06$).

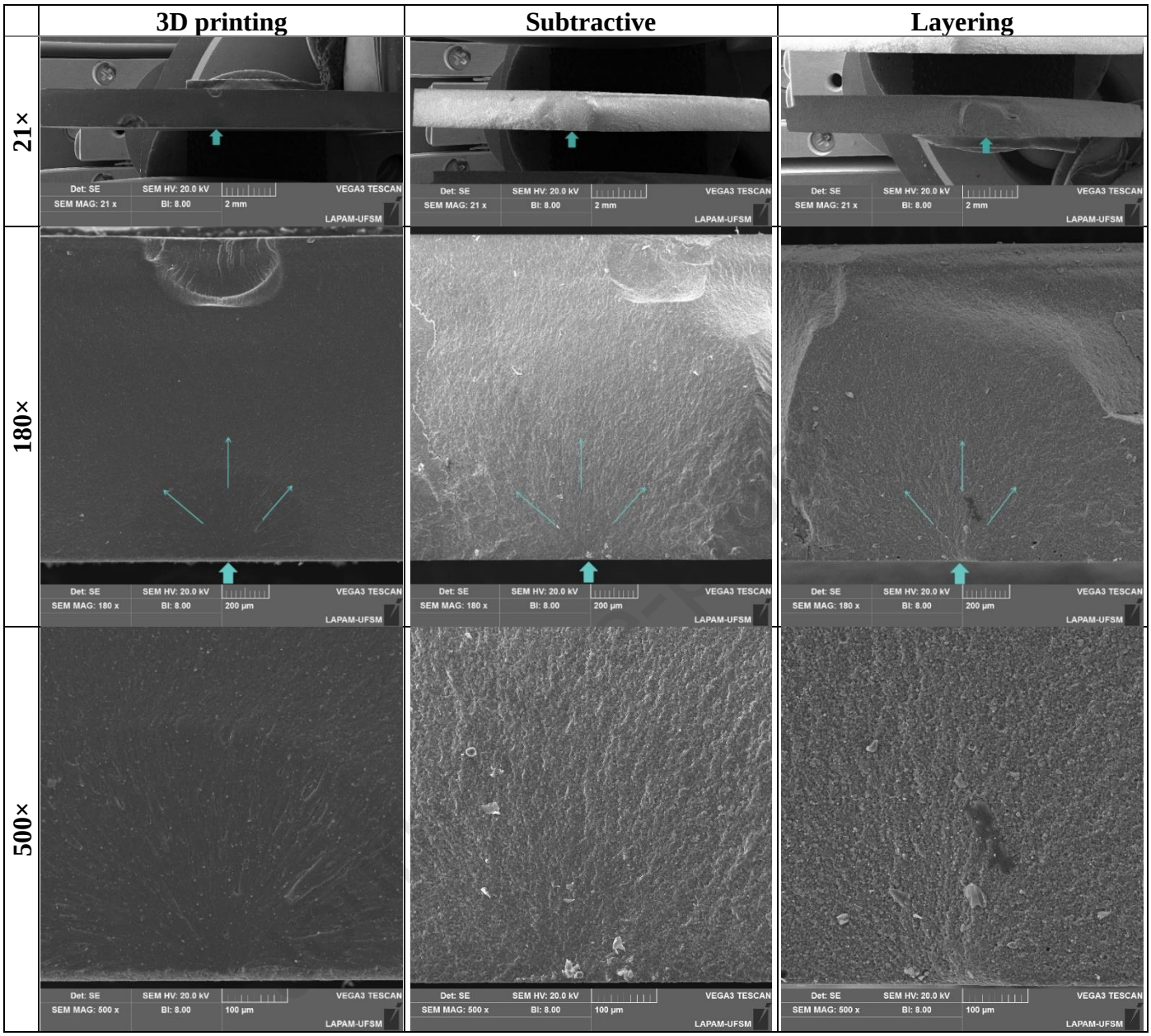

Figure 3. Representative SEM images of fractured surfaces from specimens after fatigue testing. Solid blue arrows highlight the fracture origins, pinpointing areas of tensile stress concentration during mechanical loading, while thin blue arrows denote the direction of crack propagation. These images reveal that fractures consistently originated from surface defects within regions of tensile stress concentration across all groups.

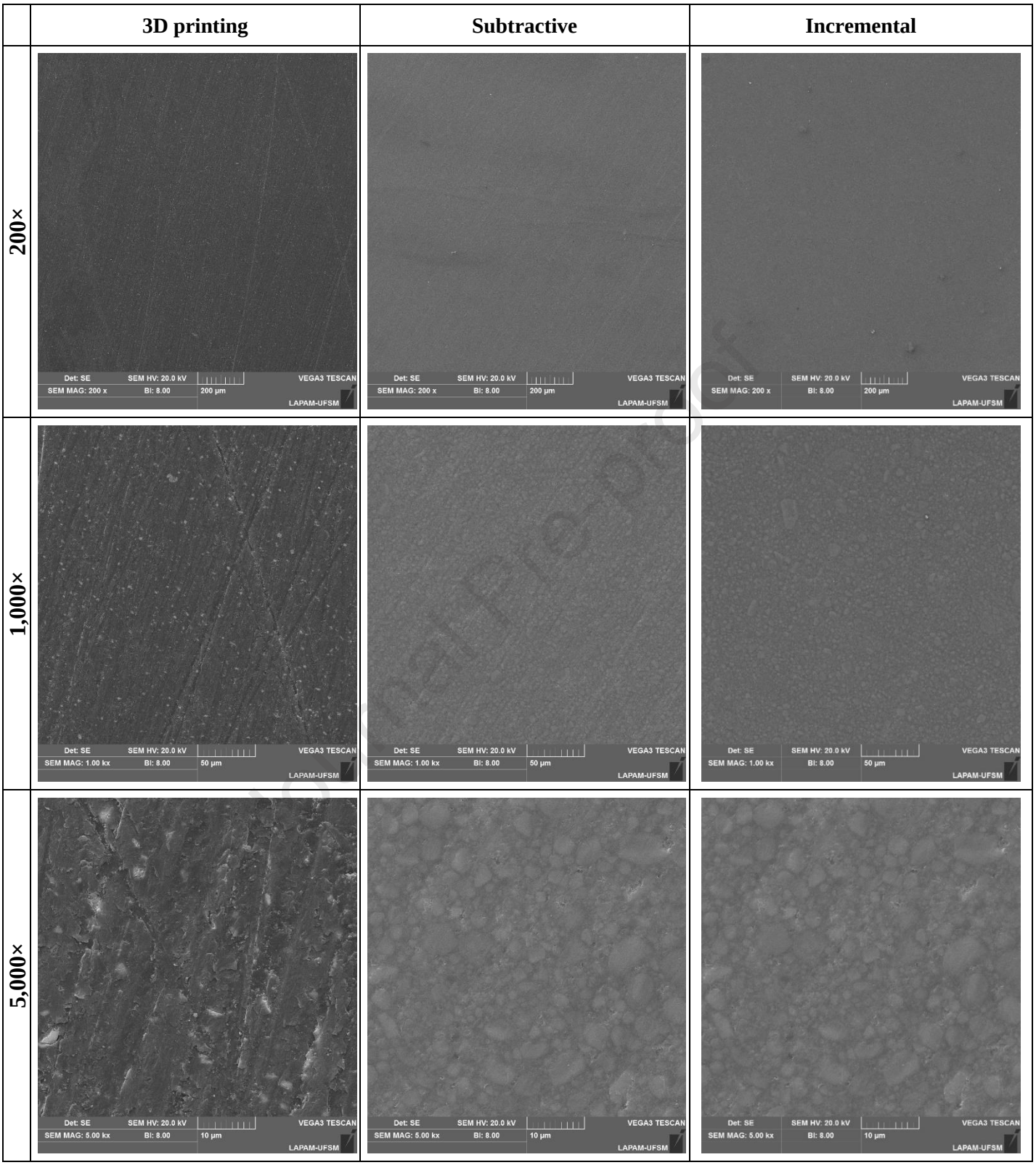

Figure 4. SEM micrographs depicting the surface topography of resin composite specimens. An irregular and porous surface is evident in the 3D Printing group, contrasting with the more compact surfaces and visible filler particles in the Subtractive and Layering groups. Despite the overall smoother appearance, minor surface defects are discernible in both of these groups as well.

Declaration of interests

☒ The authors declare that they have no known competing financial interests or personal relationships that could have appeared to influence the work reported in this paper.

☐The authors declare the following financial interests/personal relationships which may be considered as potential competing interests: